Research Article

Impact of fuel injection pressure on GDI engine performance: a numerical study with pre-combustion chamber

S Muthukumar[1*], E James Gunasekaran[2] and P Ramesh[3]

Research Scholar, Department of Mechanical Engineering, Annamalai University, Tamil Nadu, India-608002[1]
Professor, Department of Mechanical Engineering, Annamalai University, Tamil Nadu, India-608002[2]
Associate Professor, Department of Mechanical Engineering, Annamalai University, Tamil Nadu, India-608002[3]

Abstract
The automotive industry needs to develop engines with higher efficiency and lower emissions. Gasoline direct injection (GDI) engines address these demands, with better fuel economy and reduced carbon dioxide (CO_2) emissions, but face challenges in optimizing combustion processes and fuel injection strategies. The purpose of this study is to examine the combined impact of injection and pre-chamber design parameters on both pre and main-chamber combustion in order to achieve improved engine performance and emissions. Previous studies suggested that the 2% pre-chamber model achieved better combustion performance than both the standard engine (without a pre-chamber) and the 5% pre-chamber model. Therefore, in this study, a 2% pre-chamber model was numerically tested using computational fluid dynamics (CFD) codes available on the STAR-CD platform with three distinct injection pressures (IPs): 150 bar, 100 bar, and 50 bar (standard). The objective was to examine the combined impact of these pressures on mixture formation during the suction and compression strokes, as well as on combustion and emission formation. The outcome of the research reveals that the 100-bar model had superior fuel evaporation and produced a more homogenous mixture in comparison to the other two models. The same model recorded the highest peak pressure, and the difference in pressure between the three IP models was minimal. The formation of carbon monoxide (CO) increased with increasing IP during the combustion, with CO_2 formed almost similar for all three cases. The development of nitrogen oxide (NO) is lesser for both 100 and 150-bar IPs when compared to the standard IP model, whereas soot formation was negligible for all three IP models. From the study, it is concluded that the engine with 2% pre-chamber volume and 100 bar IP model yielded better performance than the standard IP model.

Keywords
Gasoline direct injection, Pre-chamber combustion, Fuel injection pressure, Engine performance, Emissions formation.

1.Introduction
Improving energy efficiency and reducing pollution levels have been prioritized globally in recent years as limits on carbon dioxide (CO_2) and pollutant emissions have been stringent [1, 2]. A lean-burn engine significantly increases thermal efficacy and, at the same time, lowers oxides of nitrogen (NO_x) emissions [1]. This is due to the excess air-fuel ratio raising the particular heat ratio and resulting in a combustion temperature lower than the one given by the stoichiometric ratio [2]. In addition, the lean-burn engine can be operated with a wide-open throttle irrespective of load conditions, lowering pumping loss and enhancing the thermal efficacy of the engine [3].

Conversely, as the charge becomes leaner, the combustion deteriorates due to some attributes, such as insufficient ignition energy and a decrease in flame velocity, leading to slow and incomplete combustion [4]. The drawback of low ignition energy can be overcome by the addition of hydrogen (which requires a low ignition energy of 0.2 mJ) [5], the use of high-energy sources such as laser or plasma ignition [6, 7], advanced combustion techniques [8], and turbulent jet ignition (TJI) [9].

Among these, recently, TJI, which is also known as pre-chamber combustion technology, has been observed as among the most promising technologies for achieving stable lean-burn combustion as well as low emission in engines. Using a pre-chamber, a flame is produced; when it is passed into the main chamber via a small hole, it ignites the lean mixture

---

*Author for correspondence

(air-fuel ratio (λ) up to 2.0) efficiently at multiple points [5]. The flame jet with highly reactive combustion products serves as a source of dispersed energy to start a combustion process. The pre-chamber technology was practically implemented by car manufacturers in the late 1970s [6]. But later, this technology became obsolete from the market due to an increase in hydrocarbon (HC) emission, heat loss, and vehicle cost caused by the incorporation of pre-chamber [7]. Further, at that time, experimental research was proven to be costly and time-consuming, which limited the research activities on the improvement of pre-chamber technology. However, the recent evolution of numerical codes to model the physics and the computer power creates an opportunity to solve those codes and to come up with a new or improved pre-chamber design at a lesser cost and time compared to experimental testing methods [8, 9]. The prechamber ignition mechanism involves the coupling of various complex phenomena like flame-wall interaction, turbulence, quenching, and reaction rate [10, 11]. Understanding these phenomena is the key to achieving an optimized pre-chamber design.

Understanding the influence of fuel IP on gasoline direct injection (GDI) engines with pre-combustion chambers lead to significant advancements in engine design. The insights gained from this study could contribute to the development of more efficient and environmentally friendly engines, aligning with global efforts to reduce the automotive sector's environmental footprint. This background sets the stage for a comprehensive numerical investigation into the effects of fuel IP on the performance of GDI engines with pre-combustion chambers, highlights the importance of optimizing this parameter for future engine technologies.

The aim of the study is to investigate the impact of fuel IP in conjunction with a prechamber design so as to achieve improved engine performance and curtailing the emissions. Therefore, in this study, a 2% pre-chamber volume model is taken and tested numerically with computational fluid dynamics (CFD) codes available in the STAR-CD platform under three various fuel IP of 50 (standard), 100 and 150 bar to study its effect on the mixture formation during suction and compression stroke, combustion, and emission formation.

The manuscript is organized as follows: Section 2 reviews the literature on various parameters of pre-chamber design. Section 3 discusses the methods adopted in this study to support pre-chamber design. Section 4 presents the results and their interpretation, while section 5 includes the discussion on study's key findings and finally section 6 concludes and also provide recommendations for future research.

2.Literature review

In recent years, extensive research has been conducted on pre-chamber combustion techniques due to their potential for improving engine efficiency, reducing emissions, and enhancing combustion stability, especially in lean-burn engines. Numerous experimental and numerical studies have explored various aspects of pre-chamber design, ignition mechanisms, and the complex interplay between combustion dynamics in the pre-chamber and main chamber. This literature review highlights key contributions in the field, focusing on turbulent jet ignition (TJI), optical diagnostics, and the influence of design parameters such as orifice diameter, ignition location, and pre-chamber geometry on combustion performance. Despite the advancements, further investigation is required to fully understand the combined effects of injection parameters and pre-chamber design for optimizing combustion efficiency.

Validi et al. [12] performed TJI combustion with a significant eddy simulation and identified three jet phases, namely turbulent hot jet, cold fuel jet, as well as reverse jet (i.e., products from main to pre-chamber). Further, they noted that the attributes of turbulent jet and combustion in the main chamber are strongly impacted by pre-chamber ignition location. Igniting the mixture close to the nozzle reduces the flow back of the unburnt mixture to the main chamber which results in better combustion in the pre as well as in the main chamber. Sadanandan et al. [13] proves that hydroxide - planar laser induced fluorescence (OH-PLIF) in a vacuum chamber in order to observe the study that the air-fuel mixture in the main chamber which is ignited by the prechamber jet tip and not by the jet's lateral sides, because of the variation in mixing behaviours. Tang et al. [14] used optical diagnostics to visualize the pre-chamber jet and the reaction zone in the main chamber at global excess air-fuel ratios (λ) of 2.3 and 1.8, respectively. They discovered that the pre-chamber jet penetration length is longer than that of the reaction zone during pre-chamber discharge; the penetration length difference between the pre-chamber jet and reaction zone decreases while increasing main chamber fuelling. Biswas et al. [15] made an investigation using Schlieren & chemiluminescence imaging

techniques in a test chamber to examine the ignition system of methane/hydrogen-air mixture by hot jet from the prechamber. They found that ignition occurred either by jet ignition or flame ignition (wrinkled turbulent flames). Further, they reported that with a rise in initial pressure and orifice diameter, the ignition mechanism is dominated by flame ignition.

When it comes to the real engine with prechamber, Attard and Parsons [16] reported that SI engines operate with pre-chamber combustion at a speed of 1500 rpm and 3.9 bar indicated mean effective pressure (IMEP) results in indicated thermal efficiency of 42% with near zero NOx emission. In another study, Attard et al. [17] claimed that the engine achieves stable combustion with a high mass fraction dilution of 54% by the incorporation of prechamber, and the fuel economy is improved by 18%. In addition, they discovered that a TJI system had shown capabilities for extending the knock limit and thereby enabling the use of gasoline with a low octane rating. By examining the spark plug location in the prechamber, Thelen et al. [18] saw that locating the spark plug away from the orifice results in better ignition and a faster combustion rate in the main chamber. Bunce et al. [19] and Jamrozik et al. [20] found that pre-chamber orifice diameter has a vital impact on the turbulence intensity in the main chamber. The smaller the diameter greater the turbulence, whereas a very small diameter hurts the main chamber combustion, leading to misfire. The studies [21–23] reported the design parameters of the pre-chamber has a vital impact on the complex combustion phenomenon both in the prechamber and main chamber.

There are many simulation studies carried out on prechamber combustion. Pielecha [24] conducted simulation analyses using AVL FIRE software to examine the effect of the air excess coefficient in the prechamber on the combustion process of a single-cylinder engine. They discovered that the combustion of global lean mixtures is effective when this process is initiated in the prechamber with a stoichiometric charge. Kim et al. [25] compared the Reynolds averaged Navier stokes (RANS) simulations with the multi-zone well-stirred reactor (MZ-WSR) and G-equation models to model combustion in lean-burn natural gas engines. They showed that while the MZ-WSR model overestimates early flame growth duration, it matches main-chamber combustion rates. The G-equation model accurately simulates pre-chamber combustion but underestimates main-

chamber rates under ultra-lean conditions, indicating a need for model improvements. Baratta et al. [26] examined the effects of cylinder head geometry and optimized the compression ratio (CR) through steady-state and transient simulations and extensive experimental testing. They found that the engine configuration with a mask showed a 20-30% decrease in the average discharge coefficient and an approximate 200% increase in the tumble ratio at partial load. With the mask at 2000 rpm and 4 bar, the tumble number and turbulence intensity increase by around 90% and 10%, respectively. Shin et al. [27] investigated the combustion and emission characteristics of a pre-chamber combustion system for heavy-duty engines using CFD simulations. At 720 rpm and 100% load, the optimal design had a 2.4 cm hole diameter, 4 holes, and a 60-degree angle. It increases gross IMEP by 0.8% and reduces total hydrocarbon (THC) and NOx emissions, but worsened NOx in dual-fuel and soot in diesel modes. Future work is suggested to develop operating strategies for these systems. Bigalli et al. [28] investigated the combustion process of a 4-stroke, gasoline SI, port fuel injection (PFI) engine equipped with a passive pre-chamber through three-dimensional(3D) CFD analysis The study involved altering the shape of the pre-chamber body and the size of pre-chamber orifices. The researchers discovered that the biggest openings generate high-velocity, heated jets of flame, which led to a 20% decrease in combustion speed and a 5% reduction in the maximum pressure within the cylinder, compared to alternative pre-chambers. Baratta et al. [29] focused on developing a high-performance spark ignition (SI) engine optimized for natural gas, featuring a high volumetric CR and variable valve actuation. It explores the impact of cylinder head geometry and CR through steady-state and transient simulations, alongside extensive experimental testing. Key findings include significant improvements in tumble ratio and turbulence intensity with mask configurations, and a reduction in combustion duration by up to 50% at specific conditions. A CR of 13 was determined as optimal, balancing combustion variability, engine performance, and fuel efficiency across different operating loads.

Though several research studies have been available on pre-chamber combustion techniques, there are still a lot of scopes for improvement that are yet to be investigated. Especially, the analysis of the combined influence of injection parameters (like injection pressure (IP), injection timing, duration, split-type)

and prechamber design (volume, nozzle diameter, length, orientation, etc.) parameters on the pre as well as main chamber combination is still limited. In the previous study [30], researchers numerically tested the four-valve SI engine with a prechamber of two different volumes (2% & 5% of clearance volume) by keeping all other parameters to a standard value and found that the 2% model gives better combustion in the main chamber than the 5% one. The current research builds on these findings by examining how different fuel injection pressures affect the combustion performance in a 2% pre-chamber volume model, aiming to provide deeper insights into optimizing pre-chamber combustion systems for real-engine applications.

3.Methods
3.1Engine computer aided design (CAD) model
The engine's 3D model was created using Catia CAD modelling software, featuring a pre-chamber volume equal to 2% of the engine's clearance volume. The engine used for analysis is a 4-stroke, single-cylinder, 4-valve, and pent-roof GDI engine. *Figure 1* depicts the CAD model of the engine. The engine design and dimensions are taken from the study of Kim et al. [31] and presented in *Table 1*. The CAD model of in-cylinder flow engine geometry is developed from the data available in the literature [30] through CATIA

V5 R19 software. The research work starts with a profile prepared on a sketcher workbench which reveals bore diameter of the cylinder and the height of the dome from the fire deck position. Then it is brought into the solid model by the shaft tool in the part model workbench. By creating a plane on both sides of the engine geometry the profile is created which denotes the trajectory path of the port and valve guide. Through part model workbench with multi-section pad option tool, the solid portion of port geometry is developed. The profile of the valve is created on both sides of the plane as in engine geometry referred to in literature in the sketcher workbench. They develop four valves through groove tool in part model workbench. The position of the piston crown was fixed as the top dead centre (TDC) by the nomenclature of the analysis software. Finally, the solid model is exported to initial graphics exchange specification (IGES) format to prepare surface mesh in STAR-CD and this further involved preparing a simulation model.

Table 1 Engine dimensions

| Parameters	Values
Bore & Stroke (mm)	86 (Square engine)
Engine Displacement (cm^3)	499.5
CR	9.2
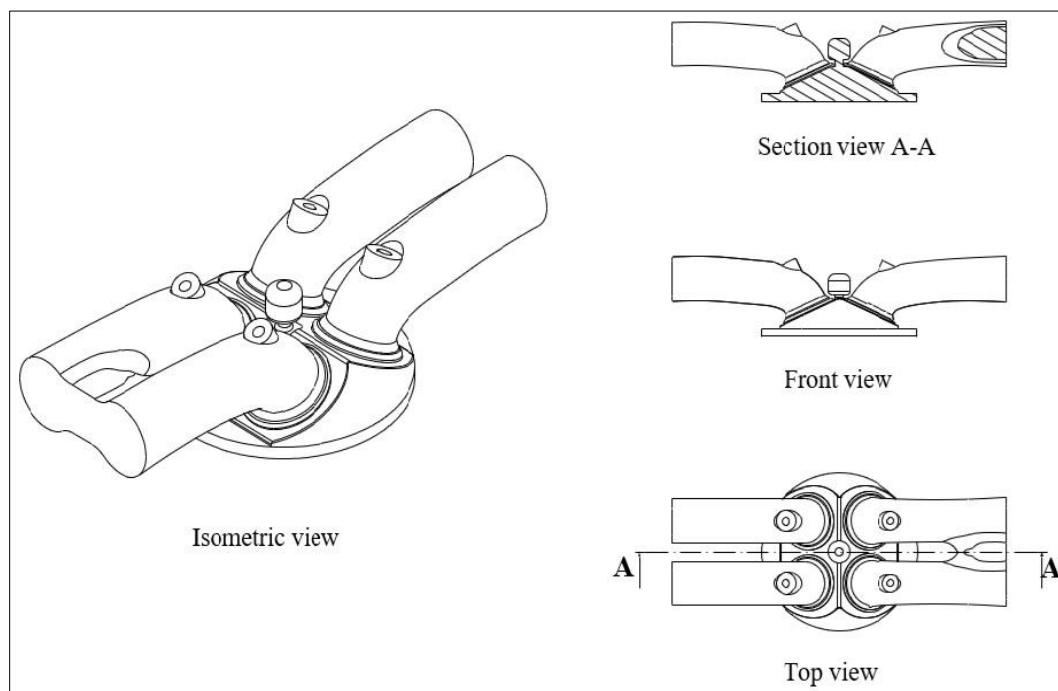
Figure 1 Engine prechamber design

3.2Surface preparation and meshing

The engine CAD model saved in the IGES format is imported into the pro-surf module of the STAR-CD to remove surface errors and generate surface mesh for the model. The software version used is CATIA V5 R19 as perpetual software and STAR-CD 4.22. The surface errors, which include duplicate edges, open edges, holes, and facets occur due to the conversion of the 3D model into a surface model when transferred from CAD to another CAE. These errors lead to the formation of surface mesh with voids. Therefore initially, these errors are repaired, and subsequently, the surface mesh is generated with a value of 0.7 and 0.05 for minimum triangulate and curvature length at the curved surface, respectively, while, at flat surfaces, a value of 5 is assigned to minimum triangulate length. *Figure 2* shows block diagram of complete work mechanism.
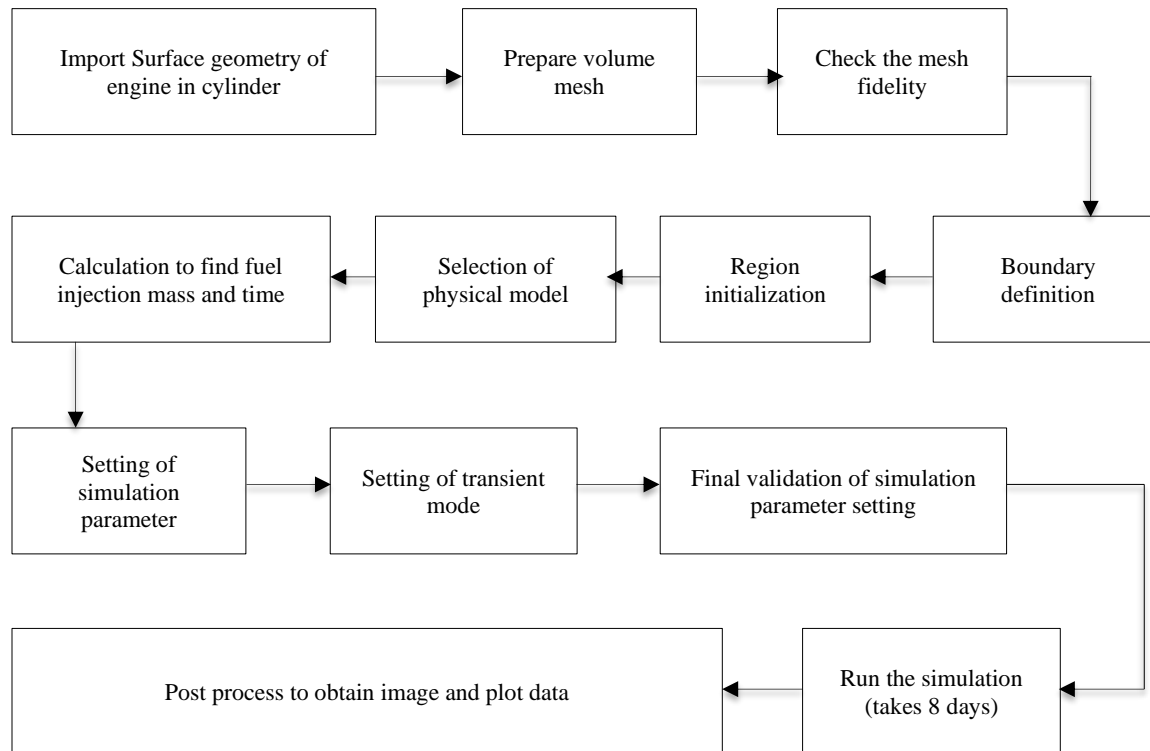
Figure 2 Working mechanism block diagram

Then the surface mesh generated model is imported into the es-ice module to generate 3D mesh and algorithm for dynamic mesh layering during piston motion. After this, the generated 3D meshes are screened to avoid any negative volume mesh in the model; otherwise, it would prevent the simulation from running. In addition, an auto-mesh operation is activated to activate and deactivate the 3D mesh layer during valve events. The valve events are given in *Table 2*. The maximum valve lift was 9 mm. The mesh structure was filled with hexahedral/trimmed meshes.

Table 2 Valve events

Timing	Events
55˚ after bottom dead centre (aBDC)	Exhaust Valve Open
10˚ after top dead center	Exhaust Valve Close

Timing	Events
(aTDC)	
10˚ before top dead center (bTDC)	Inlet Valve Open
55˚ aBDC	Inlet Valve Close

3.3Using governing equations and solver techniques for modelling physics

The model used to represent the flow field physics was called RANS, which solves the equation of state and the set of Navier-Stokes equations by combining the fluctuation component with the mean term of the flow field variables. For the variables in the flow field, the equations for continuity, energy, momentum, and transport are solved. The pressure-velocity coupling equation is solved using the pressure-implicit with splitting of operators (PISO) technique.

The two-equation RANS model re-normalized group (RNG) k-epsilon is used to simulate the turbulence in the flow field [32]. To replicate the spray process, the discrete droplet model and the continuous stage of the injector model are integrated. The Eulerian method is used to represent the continuous phase, while the Lagrangian approach is used to model the discrete phase. The atomization process is chosen to be modelled by the Reitz-Diwakar paradigm. The Reitz breakup model is observed to describe the secondary droplet breakdown, while the Bai wall impingement model with rebound criterion is employed to investigate the droplet wall contact [33]. The combustion process is modeled by the extended coherent flamelet model (ECFM) approach. The ECFM approach is more suitable for homogeneous premixed combustion [34] because this model can simulate complicated dynamics like flame propagation, turbulence mixing, and pollution emission better. In the simulation, isooctane is selected as a surrogate for gasoline. The Zeldovich mechanism (expanded) and the Hiroyasu paradigm predicted the oxides of nitrogen (NO) and soot generation. To raise the accuracy of the findings closer to the wall, the conventional wall function option is selected.

The monotone advection and reconstruction (MARS) discretization technique is utilized to resolve the U, V, and W momentum and turbulence, while the upwind scheme (UD) is employed to determine the temperature. The central differencing method is chosen to calculate density.

3.4 Initial and boundary conditions

Boundary condition is a term that express the simulation to identify the distribution of data with the surroundings. The proper setting of boundary conditions shows the stability of results and achieve the consistency of convergence. The boundary of engine geometry is defined as cylinder, ports and valves. The cylinder boundary consists of combustion dome regions, piston crown regions and cylinder wall region (liner) to assume and fix the boundary region by the value of temperature 450 K, 480 K and 400 K accordingly and the value of resistance were 0 m^2K/W. The port wall regions, the valve stem regions and valve face regions were assumed as adiabatic wall this is due to the region near the valve guide and valves were not fixed and these were moved along the axis valve axes. The boundary on the port which allowed the flux into the port are treated as inflow pressure region and the flux out of the port as outflow region. These regions are assumed as environmental

absolute pressure with constant value 101325 Pa, temperature with constant value 323 K, turbulence intensity value 5% and turbulence length scale value 1%.

The atmospheric pressure constraint is utilized at the intake and outflow borders since the engine is naturally aspirated. The clearing volume is initialized with residual gases before the commencement of the simulation to record the real state since the simulation was run for a single cycle. By taking the valve overlap duration into account, the intake port was prefilled with 5% of the remaining gases. Initial turbulence intensity is set at 5%. No-slip wall boundary condition was applied. The temperature condition applied to different boundary portions of the engine model at the different durations of the simulation is detailed in *Table 3*.

Table 3 Boundary conditions

Boundary	Parameters	Conditions	
		Suction	Both valves closed
Inlet (Intake) & Outlet (Exhaust)	Pressure	101325 Pa	-
	Turbulence Intensity	5%	-
Intake Cylinder head Piston Top Liner Inlet Valve Exhaust Valve	Temperature	323 K 450 K 480 K 400 K 400 K 450 K	- 550 K 550 K 500 K - -

The simulation is performed for a speed and load condition of 1000 rpm and 10 kW, respectively. The fuel quantity required for the corresponding load value was given as 43.98 mg/cycle, which is taken from the experimental study reported by Kim et al. [31]. The values of the other simulation parameters are presented in *Table 4*. The simulation started from 20° before the beginning of the suction stroke (i.e., 340°) and ended after the power stroke (i.e., 900°).

Table 4 Engine simulation parameters

Start of the suction stroke	360°
Start of Injection	350°
Lamda, λ	1
Start of ignition	700°

### 3.5 Grid independence study and validation
The results of the CFD model of the standard engine are validated with the experimental result of the v

component of average fluctuation velocity given by Kim et al. [31]. The CFD findings are initially validated with the experimental one. It is found that the result of the model with 235449 grid cells is in good agreement with experimental results with some discrepancies near the suction TDC. The Grid independence study is discussed in the previous study [30].

4.Results

4.1Influence of fuel injection pressure on in-cylinder mixture distribution

The preparation of the mixture plays an important role in achieving an efficient engine with complete combustion. Changes to the induction route and valve design result in different fluid velocities inside the cylinders, which affects the formation of the mixture. *Figure 3* indicates the variation in charge induction during the suction and compression stroke. There is a small dip in the charge induction at the start of the suction. This is due to valve overlapping, which allows a few quantities of fresh charge to escape through the exhaust valve. Thereafter the variation in induction is linear up to 500-degree crank angle (°CA) and then becomes non-linear up to 590°CA. A sudden dip is seen at 593°CA, indicating that there is an escape of mixture through the intake valve during compression, as the inlet valve closes 55°CA aBDC. After this, there is no variation with the charge induction trend showing a straight line. All three IP cases have shown the same trend of charge induction.
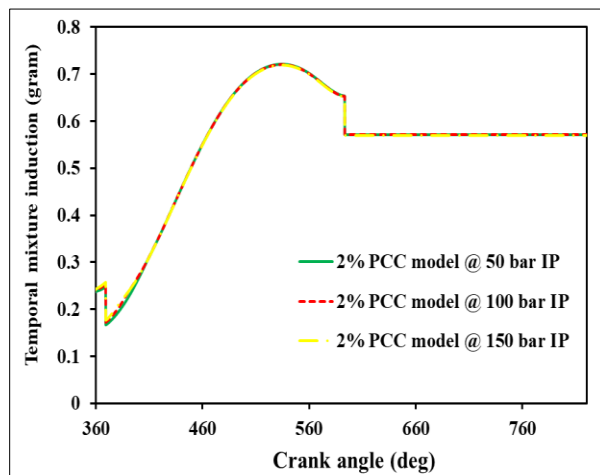
Figure 3 Variation in charge induction

Table 5 shows the contour plot for air-fuel mixture formation and distribution w.r.t.CA positions for three pressure conditions. Fuel injection duration is varied between 350° and 400°CA for all three test

conditions. On the basis of mixture, it is defined by three modes, namely rich ($\Phi>1$), homogeneous ($\Phi=1$), and lean ($\Phi<1$). It is observed that the mixture is highly rich during the fuel injection period, and it continues up to 440°CA.

Figure 4, which gives temporal rich mixture percentage w.r.t. crank position, also shows that the percentage of rich mixture formation increases with increasing IP and achieved a maximum of 60% and 64% at a crank position closer to 450°CA for 100 and 150 bar IP cases, respectively. Whereas for standard IP, the maximum percentage of rich mixture formation observed is 46%, which occurs 30°CA later than that in the other two IP cases. The reason is that with higher IP the mean droplet size reduces shown in *Figure 5* and hence improves evaporation rate as shown in the *Figure 6*, which indicates that 150 bar IP, the sauter mean diameter (SMD) of droplets almost becomes zero by the 395°CA, when compared with 100 bar IP, where by 405°CA the droplets almost evaporated.
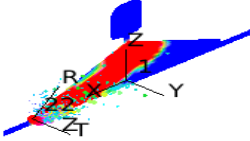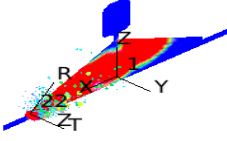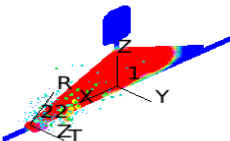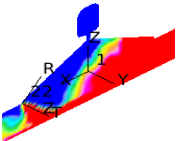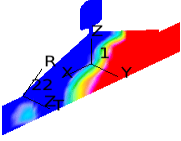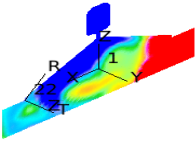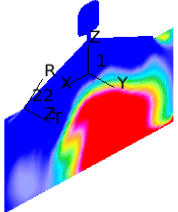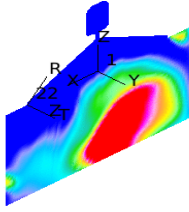
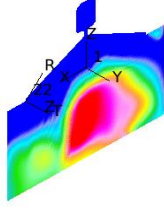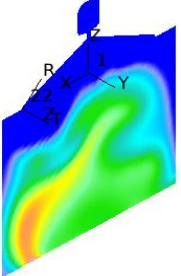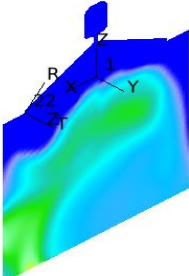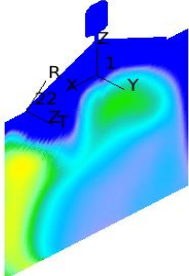Furthermore, as the fuel injection duration decreases with increasing IP, the quantity of fuel (i.e., number of droplets) introduced during the early part of the suction stroke increases. Hence, the rich mixture formation is initially higher for higher IP cases when compared to standard IP. Conversely, *Figure 7* displays that the mass of fuel vapor with respect to °CA increases with IP. This indicates that the conversion of liquid fuel into vapor is faster at higher IPs. This is due to a decrease in SMD with an increase in IP. As the diameter decreases, the surface-to-volume ratio increases, which in turn raises the evaporation rate and findings in a higher quantity of fuel vapours. Therefore, after 460°CA for 100 and 150 bar IP and after 480°CA for 50 bar IP, the rich mixture distribution decreases gradually, and the air-fuel mixing phase starts to take place at a rapid pace. As a result of this, the mixture tends to become homogeneous and lean. It is inferred from the contour plot that the formation of a homogenous mixture is faster in the case of 100 bar IP when compared to the other two cases.
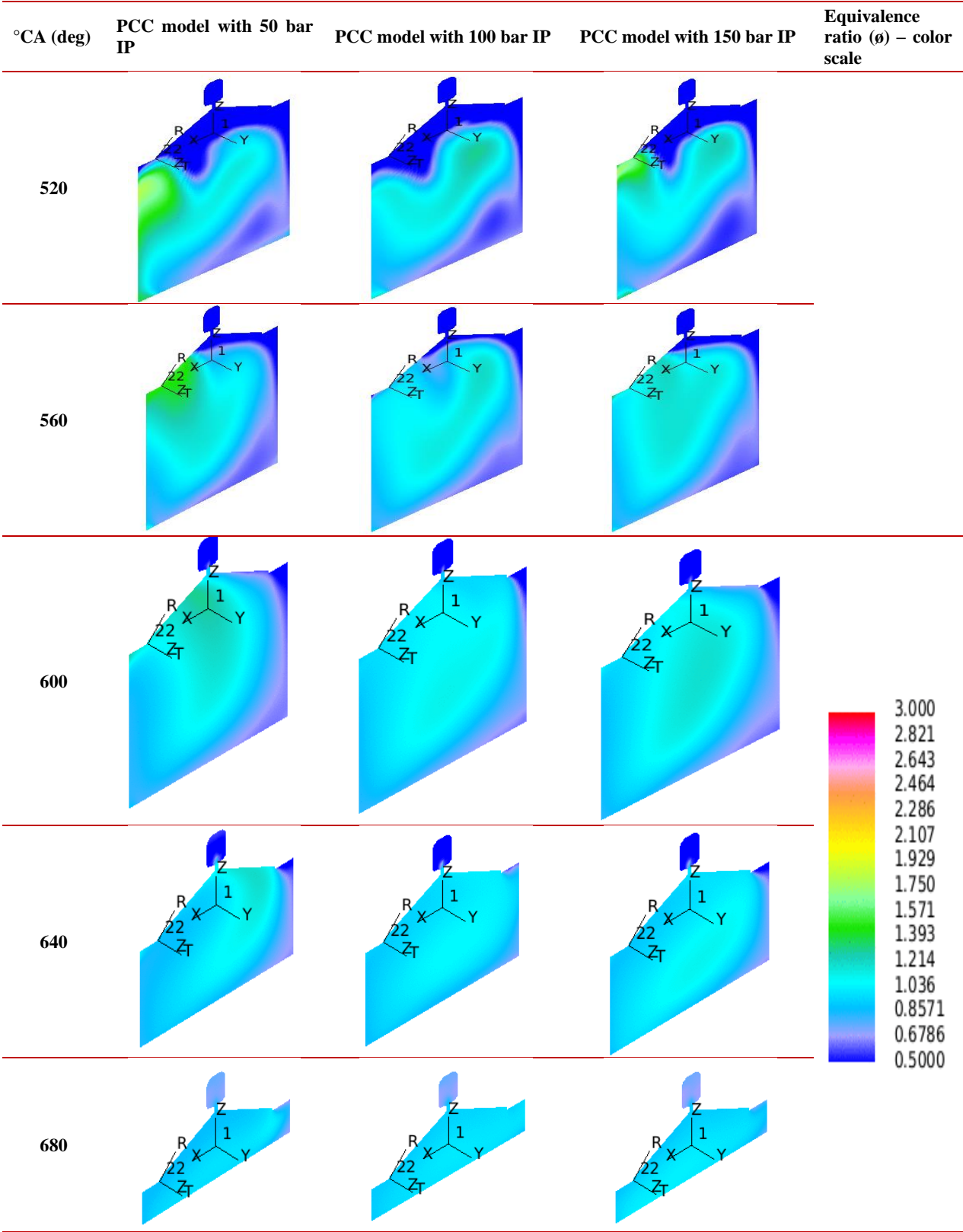
From *Figure 8*, the proportion of homogenous mixture formation just before the start of ignition is found to be highest for the 100 bar IP (~98%) model, followed by 150 bar (~94%) and standard IP (~84%). The reason is that as the IP rises, the injection rate increases which shorten the injection duration and gives more time for the injected fuel to evaporate and form a proper air-fuel mixture. In addition to this, the
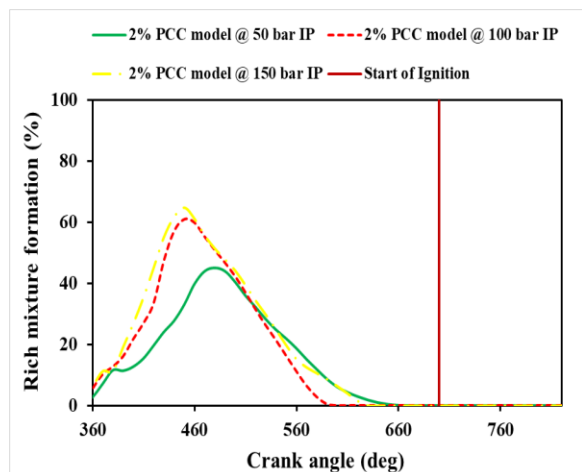
turbulence induced by the fuel jet during the fuel injection process increases with an increase in IP. This increase in turbulence further enhances the mixing process which in turn improves the mixture formation and outcomes in a more homogeneous mixture throughout the cylinder. *Figure 9* shows that the percentage of lean mixture distribution is negligible for 100 and 150-bar IPs and is around 15% for standard IP at 700°CA. It is observed that the percentage of lean mixture formation is negligible for the 100 bar IP model, whereas for 150 bar, it is around 5% at the point just before the start of ignition. The reason for the increase in lean mixture formation at 150 bar IP is owing to over mixing of fuel and air which is caused by the additional turbulence induced by an increase in IP. At the beginning of ignition, there is no rich mixture formation in all three IP cases. Comparing the mixture formation process of all three IPs, the 100 bar IP results in better and homogenous mixture formation.
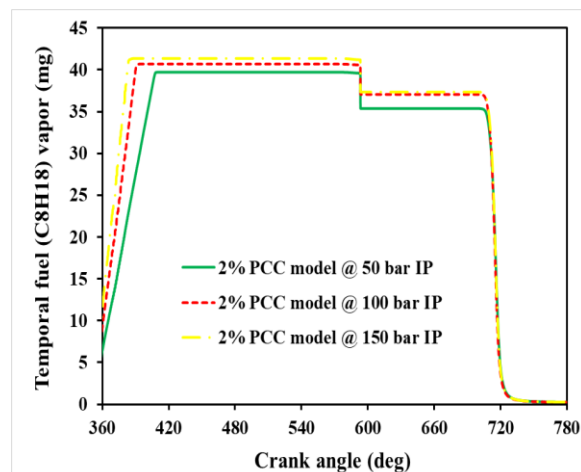
Table 5 Mixture formation at different °CA

°CA (deg)	PCC model with 50 bar IP	PCC model with 100 bar IP	PCC model with 150 bar IP	Equivalence ratio (ø) – color scale
360				
400				
440				
480				

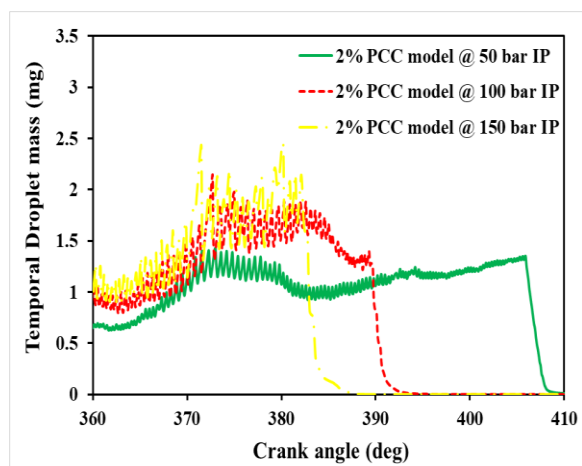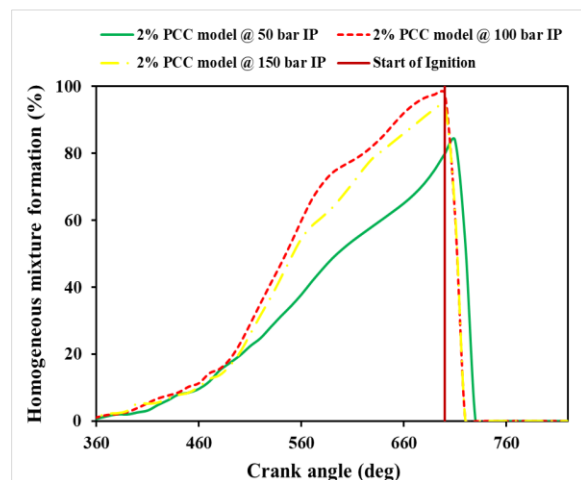| °CA (deg)	PCC model with 50 bar IP	PCC model with 100 bar IP	PCC model with 150 bar IP	Equivalence ratio (ø) – color scale
520				
560				
600				3.000 2.821 2.643 2.464 2.286 2.107 1.929 1.750 1.571 1.393 1.214 1.036 0.8571 0.6786 0.5000
640				
680				

Figure 4 A rich mixture of character within the cylinder

Figure 5 Droplet mass during fuel injection

Figure 6 Average SMD w.r.t. CA position

Figure 7 Charges in the vapor formation state

Figure 8 Homogeneous mixture character within the cylinder
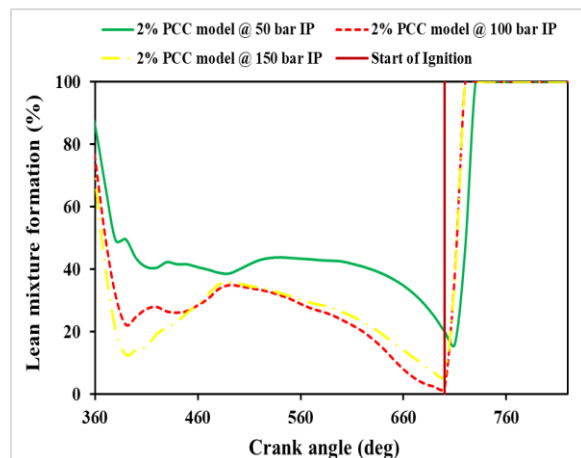
Figure 9 Lean mixture character within the cylinder

4.2 Impact of fuel injection pressure on combustion characteristics

Figure 10 displays the variation of pressure during combustion for all three pressure cases, along with the motoring curve. The rising pressure mainly depends on how fast the combustion takes place after the point of ignition. One of the factors that decide the pace of the combustion is the rate of flame propagation. The in-cylinder pressure with respect to °CA appears to be slightly higher for 100-bar and 150-bar IP cases when compared to standard IP cases. Among the tested IPs, the 100 bar IP displays a faster rise in pressure and results in maximum peak pressure. This is due to increased flame speed as the IP is increased from 50 to 150 bar, which is also confirmed by the mass of fuel burnt trend as shown in *Figure 11*. Compared to standard IP, the mass of fuel burnt is higher for both 100-bar and 150-bar cases with the former being marginally higher than the latter. This is because the air-fuel mixture formed before the start of ignition is more homogeneous throughout the cylinder at higher IPs. Generally, the flame speed is higher in the homogeneous mixture when compared to the lean and rich mixture. As the 100-bar case comparatively shows more homogenous (see *Figure 11*) mixture formation, it shows increased flame speed, leading to combustion enhancement and thus increasing the in-cylinder pressure.

Furthermore, *Table 6* and *Figure 12* show the variation in combustion temperature w.r.t. CA using contour and line plots, respectively. It is found from the plot of the contour that the temperature distribution pattern seems to be almost similar, with the high-temperature region within the contour slightly higher for 100 and 150-bar IP cases. This is also inferred from *Figure 12* that the 100 and 150-bar IP cases show a slightly higher temperature w.r.t. CA position between 700° and 730°CA when compared to the 50-bar IP one. However, the difference in temperature between 100 and 150 IP cases is very small, with the latter being marginally inferior to the former. The reason for the slight increase in temperature at higher IPs is owing to a rise in heat release rate, which results from faster flame propagation, causing more fuel to burn per unit °CA.
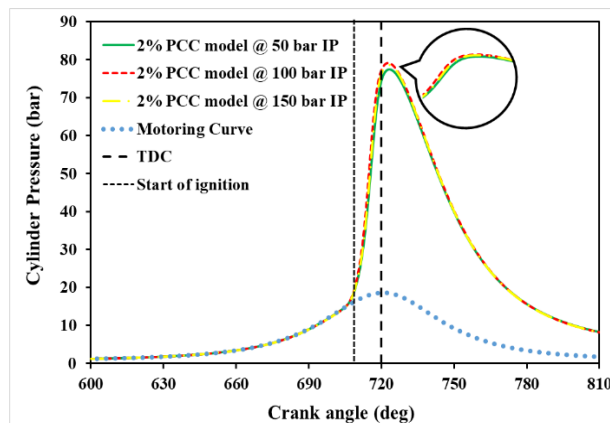

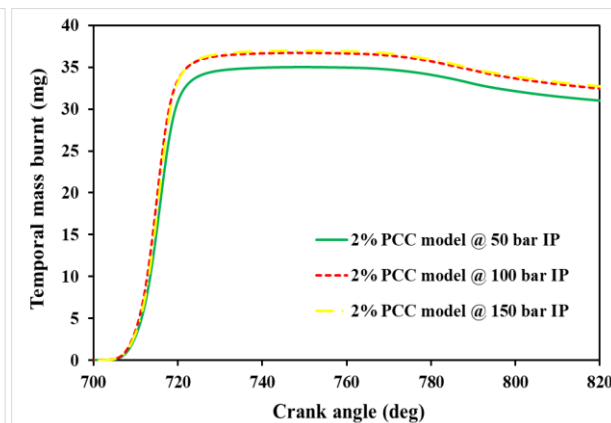**Figure 10** Modification of in-cylinder pressure


Figure 11 Mass of fuel burnt w.r.t. °CA

Table 6 Temperature distribution during combustion

°CA (deg)	PCC Model with 50 bar IP	PCC Model with 100 bar IP	PCC Model with 150 bar IP	Temperature Scale (K)
700				
710				

°CA (deg)	PCC Model with 50 bar IP	PCC Model with 100 bar IP	PCC Model with 150 bar IP	Temperature Scale (K)
720				3200. 2993. 2786. 2579. 2372. 2165. 1958. 1752. 1545. 1338. 1131. 923.8 716.9 509.9 303.0
730				
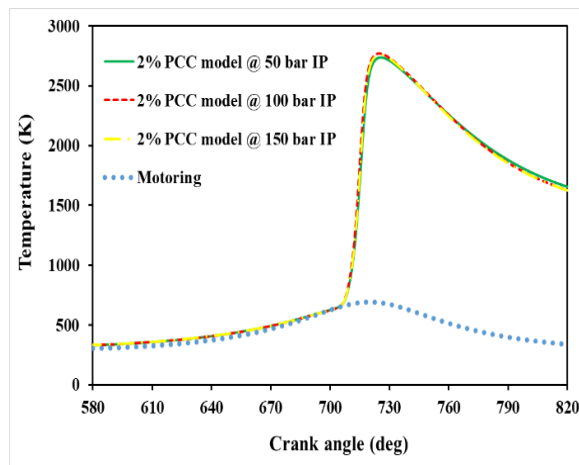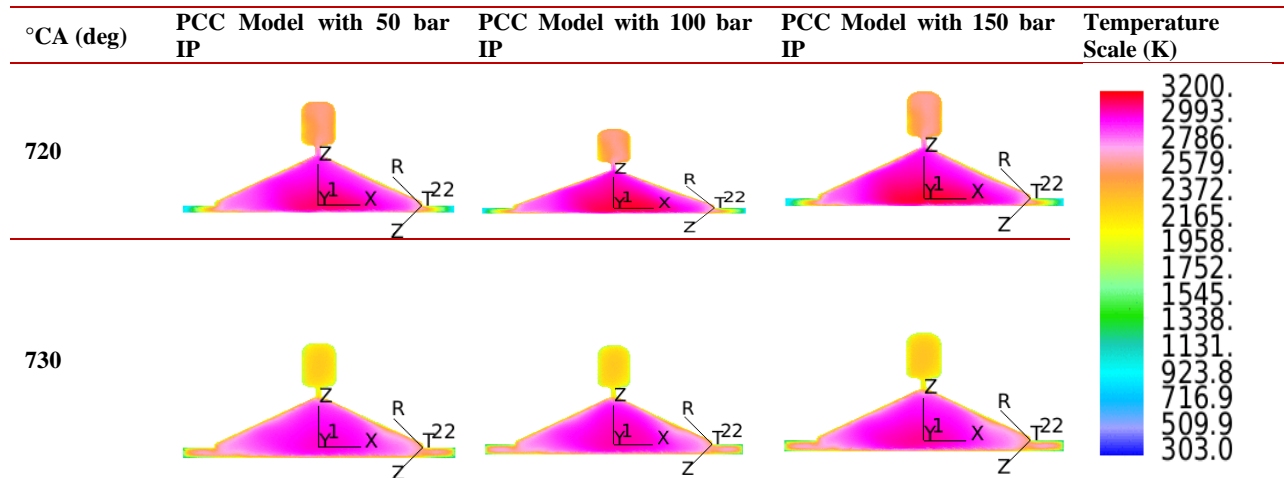
Figure 12 Variation of the temperature inside the cylinder

4.3 Impact of fuel injection pressure on emission formation

The availability of oxygen (O_2) and the formation of CO, NOx, CO_2, and soot inside the cylinder during the combustion process decides the engine end emissions. Analysing those concentrations during combustion gives a better understanding of the emission, which helps in designing a better engine module. The availability of oxygen is the key parameter that decides the combustion quality and formation of other toxic emissions. *Figure 13* shows temporal oxygen variation during suction and compression stroke. All three IP cases have the same amount of oxygen.

The CO formation increases when the IP is increased from 50 to 150 bar, as revealed in *Figure 14*. The increase in flame speed with IPs leads to faster oxidation of fuel which in turn increases the CO formation during combustion. Though CO formation is higher for 100 and 150 bar cases, they are all quickly oxidized to CO_2 due to a rise in combustion temperature. It is observed from *Figure 15* that between 710° and 720°CA, the CO_2 formation is almost similar for 50 and 150 bar IP cases, whereas it is marginally higher for the 100 IP model. After 720°CA, the CO_2 trend decreases while increasing IP. However, the difference between the IP cases is very small.

Furthermore, the generation of NO initially is similar for all three cases, but later, the standard IP case showed higher NO formation than the other two, as presented in *Figure 16*. The increase in flame speed raises the fuel rate burn and thereby decreases the resident time available for the NO formation. Thus, NO gets reduced as IP is raised from 50 to 150 bar. *Figure 17* compares the soot formation of all three IPs. Though the soot is relatively higher for 150 and 100 IP cases than standard IP, its concentration is negligible when compared to the total mass of the combustion products. The over-lean/rich effect locally with increasing IP due to better atomization and mixing could lead to diffusion combustion, which in turn produces soot.
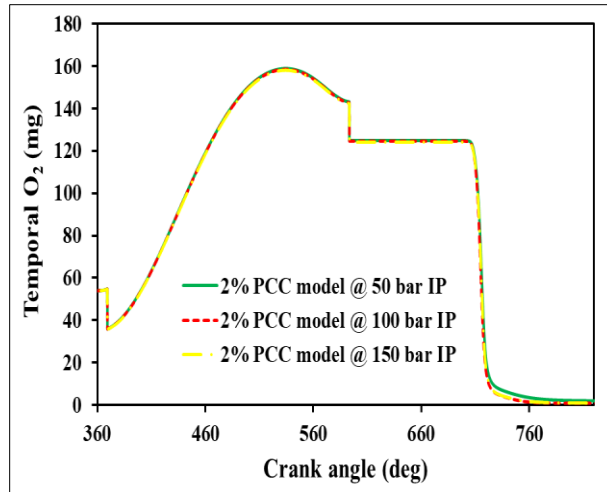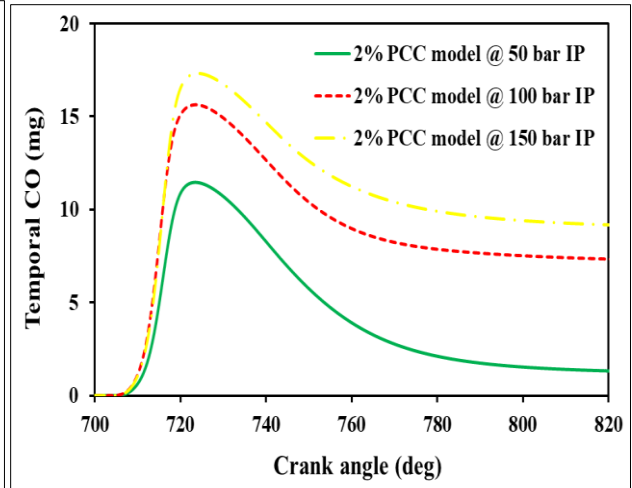
Figure 13 The amount of oxygen used in the cycle
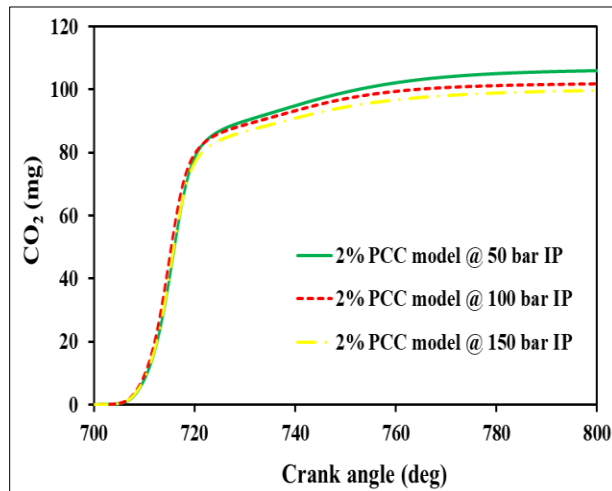

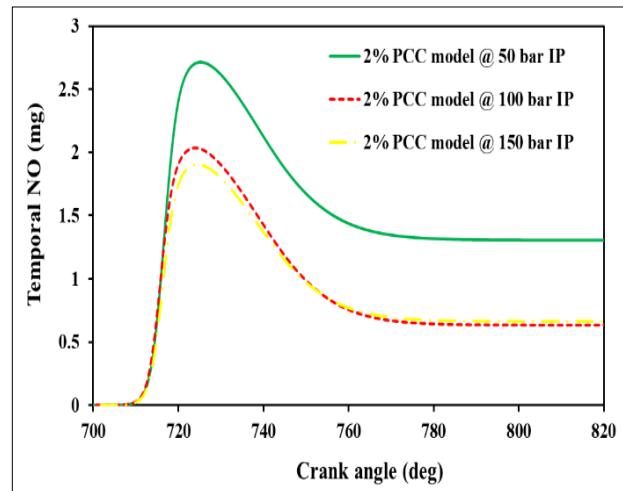
Figure 14 CO produced during combustion

Figure 15 CO_2 produced during combustion
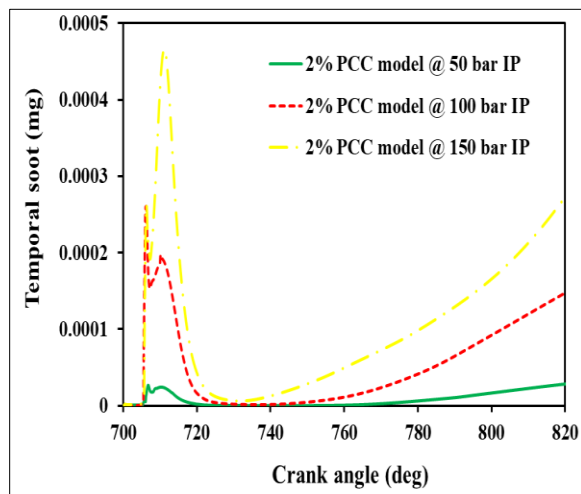

Figure 16 NO formation during combustion

Figure 17 Soot formation during combustion

5. Discussion

The result of this numerical analysis demonstrates that the fuel IP significantly affects the process of combustion and the air-fuel mixture. As the fuel IP increases from 50 to 100 bar, the air-fuel mixing process is improved, leads to a uniform distribution of the air-fuel mixture throughout the cylinder (closer to stoichiometric ratio). The main reason behind the present action is the better atomization of the fuel due to the increased IP, which leads to finer fuel droplet particles, resulting in faster evaporation and better mixing [35].

Therefore, the combustion process is enhanced and leads to a higher peak pressure and temperature compared to constant IP (50 bar). However, when the IP is increased to 150 bar, due to excessive atomization of the fuel, the mixture becomes slightly

lean/rich locally, disrupting the uniform air-fuel mixture formation [36]. This adversely affects the combustion process, causing a slight decrease in peak pressure and temperature. So, the peak pressure and temperature at 150 bar are lower than at 100 bar. CO formation shows a sharp rise owing to a rise in combustion temperature with rising fuel IP [37]. However, all three IP events result in similar CO_2 formation. NO formation decreases with increasing IP. Despite the rise in temperature with higher IP, NO emissions are reduced. This mainly occur due to faster combustion process during the better mixture formation. Thus, it reduces the residence time for NO formation [38]. As far as soot emission is concerned, it is the least in all three cases because of a decrease in the soot formation sites owing to the distribution of the air-fuel mixture closer to the stoichiometric range. The results of the current study are compared to previously published results in *Table 7*. In

comparing the combustion and emission results across the studies, the present study, Frasci et al. [39], and Lu et al. [40] all show improvements in peak cylinder pressure, soot, CO, NOx, and CO_2 emissions under optimal conditions, marked by positive trends. Specifically, the present study highlights significant enhancements at an injection pressure of 100 bar, while Frasci et al. achieve similar improvements with a 420 mm³ prechamber volume and 0.91 mm nozzle diameter. Lu et al. report optimal combustion and emission performance with a 3% prechamber volume, 2 mm nozzle diameter, and 30° inclination. In contrast, Wang et al. [41] provide no data on combustion and emission characteristics, focusing instead on nozzle geometry without detailed emission results. Overall, all studies indicate that fine-tuning parameters like prechamber volume, nozzle size, and injection pressure leads to better combustion efficiency and reduced emissions.

Table 7 Comparison of the present study with the previous studies

		Present study	**Frasci et al.** [39]	**Lu et al.** [40]	**Wang et al.** [41]
Prechamber Volume		2%	420, 600, & 780 mm³	1%, 2%, 3% & 5%	-
Engine type		GDI	Gasoline engine with PFI	Heavy-duty diesel engine	Constant volume chamber
Operating conditions		1000 rpm, 10 KW	4500 rpm, 13 bar IMEP	1200 rpm, Full load	415 K, 0.6 MPa
Experiment/ simulation (platform)		Simulation (STAR-CD)	Both	Both	Experiment
Varying parameter		IP (50, 100, & 150 bar)	Nozzle diameter (0.49, 0.7, & 0.91 mm)	Nozzle diameter (2, 4, & 6 mm) Nozzle Inclination (30°, 45°, & 60°)	Nozzle parameters 1. Diameter: 4, 7, 10 mm 2. Numbers: 4, 6, 8 3. Transition angle: 60°, 120°, 180°
Best / Optimal condition		IP - 100 bar	420 mm³ & 0.91 mm	Prechamber volume - 3% Nozzle diameter & Inclination - 2mm / 30°	Diameter: 4 mm Number: 4 Transition angle: 60°
Combustion	Peak cylinder pressure	☝	☝	☝	☝
	Peak heat release rate	Not available	Not available	Not available	☝
	Peak cylinder Temperature	☝	☝	☝	☝
Emission formation	Soot	☝	☝	☝	Not available
	CO	☝	☝	☝	Not available
	NOx	☝	☝	☝	Not available
	CO₂	☝	Not available	Not available	Not available

5.1Limitations of the study

1. The combustion model employed (ECFM approach) may not capture all the intricacies of combustion phenomena, such as turbulence-chemistry interactions and flame propagation dynamics, which could influence the accuracy of predictions related to combustion efficiency and emissions.
2. The findings in this study are derived solely from computational methods, underscoring the need for experimental validation to more accurately assess engine performance, particularly with regard to exhaust emissions.
3. The reported results are limited to a single operating condition, specifically at full load. Further research is necessary to evaluate engine performance across a broader range of operating conditions, including various speeds and load levels.

The outline of a potential experimental setup that could validate the numerical findings of the present study is given as follows:

1. Use a single-cylinder or multi-cylinder GDI engine equipped with a pre-combustion chamber which is identical to the numerical model. Ensure the engine is instrumented to measure cylinder pressure, fuel injection characteristics, exhaust emissions, and other relevant parameters.
2. Implement a setup where fuel IP can be varied systematically across a range of interest (e.g., 100 bar to 300 bar). Ensure precise control and measurement of IP using suitable high-pressure fuel systems.
3. Conduct steady-state and transient tests under various engine operating conditions (e.g., different engine speeds, loads, and fuel compositions). Measure key performance parameters such as brake-specific fuel consumption (BSFC), IMEP, combustion stability, and emissions (CO, CO_2, NO_X, HC).

5.2Practical implications of the study

The results of the study on the impact of fuel IP in a GDI engine with a pre-combustion chamber have significant practical implications for improving engine design and fuel injection strategies in real-world applications. The findings offer engineers valuable insights on optimizing fuel injection by identifying the ideal IP that balances fuel efficiency, engine performance, and emission levels. For instance, understanding the effect of different IPs on combustion stability and heat release rates can help create more efficient, lower-emission engines.

Additionally, by analysing the influence of fuel IP on key combustion characteristics such as ignition delay, flame propagation, and turbulence intensity, engineers can further optimize engine designs. This can lead to improved fuel efficiency and reduced greenhouse gas emissions, in line with stringent environmental regulations. Adjusting the fuel IP according to the research findings can effectively reduce the emission of NOx, PM, and HC, thereby minimizing pollution.

Moreover, optimizing injection parameters to improve combustion efficiency in the pre-combustion chamber can significantly reduce pollutant emissions, contributing to better air quality. The study's outcomes lay the foundation for future advancements in GDI combustion technology. By incorporating validated computational models into engine design processes, manufacturers can streamline design iterations, reduce development costs, and accelerate the introduction of innovative engine designs to the market.

A complete list of abbreviations is listed in *Appendix I*.

6.Conclusion and future work

The current research work tested the engine with a pre-chamber volume of 2% of clearance volume at three different IPs of 50 bar, 100 bar, and 150 bar. The engine with pre-chamber volumes was developed using CATIA software. Further, the IP impacts on the mixture distribution, combustion, and emission properties of an engine with a prechamber at 1000 rpm and full load were numerically examined with CFD codes included in the STAR-CD simulation software.

The primary conclusions of this investigation are as follows:

- The 100-bar model showed better homogeneous mixture formation when compared to the other two IP models.
- The peak pressure is found to be the highest for the 100-bar IP model, with minimal difference between the three IP models.
- The CO formation increased with increasing IP during the combustion. However, the formation of CO_2 is almost similar for all three cases.
- The NO formed is lesser for both 100 and 150-bar IPs when compared to the standard IP model. Both 100 and 150-bar IP models showed similar NO levels at the end of a power stroke.

Among the tested IPs, the 100-bar IP case model performs better than the other two IP cases. According to the study, engines which have a prechamber volume of 2% of the clearance volume and an IP of 100-bar can simultaneously cut emissions and enhance combustion. However, still, more analysis is required with this configuration for further improvisation of the model by advancing the spark timing, raising the CR and the air-fuel ratio (i.e., for $\lambda >1$), varying the fuel injection strategies, and optimization of the prechamber design like nozzle diameter and length, and throat diameter.

Acknowledgment
None.

Conflicts of interest
The authors have no conflicts of interest to declare.

Data availability
None.

Author's contribution statement
S Muthukumar: Conceptualization, investigation, data curation, design, data collection, modelling, analysis, writing – original draft, writing – review and editing. **E James Gunasekaran:** Data collection, conceptualization, writing – original draft, analysis and interpretation of results. **P Ramesh:** Study conception, design, data collection, supervision, investigation on challenges and draft manuscript preparation.

References
[1] Novella R, Pastor J, Gomez-soriano J, Barbery I, Libert C, Rampanarivo F, et al. Experimental and numerical analysis of passive pre-chamber ignition with EGR and air dilution for future generation passenger car engines. SAE Technical Paper. 2020:1-18.

[2] Distaso E, Amirante R, Cassone E, Catapano F, De PP, Sementa P, et al. Experimental and numerical analysis of a pre-chamber turbulent jet ignition combustion system. SAE Technical Paper. 2019.

[3] Peters N, Subramanyam SK, Bunce M, Blaxill H, Cooper A. Optimization of lambda across the engine map for the purpose of maximizing thermal efficiency of a jet ignition engine. SAE International Journal of Advances and Current Practices in Mobility. 2020; 2:3140-50.

[4] Russwurm T, Schumacher M, Wensing M. Active fuelling of a passenger car sized pre-chamber ignition system with gaseous components of gasoline. SAE Technical Paper. 2020:1-11.

[5] Tian J, Cui Z, Ren Z, Tian H, Long W. Experimental study on jet ignition and combustion processes of natural gas. Fuel. 2020; 262:116467.

[6] Alvarez CE, Couto GE, Roso VR, Thiriet AB, Valle RM. A review of prechamber ignition systems as lean combustion technology for SI engines. Applied Thermal Engineering. 2018; 128:107-20.

[7] Dale JD, Checkel MD, Smy PR. Application of high energy ignition systems to engines. Progress in Energy and Combustion Science. 1997; 23(5-6):379-98.

[8] Macián V, Salvador FJ, De LMJ, Pagano V. Combustion analysis of a stratified pre-chamber ignition system by means of a zero-dimensional turbulence and flame speed model. Combustion and Flame. 2021; 232:111526.

[9] De BV, Malfi E, Bozza F, Kumar D, Serrano D, Dulbecco A, et al. Experimental and 0D numerical investigation of ultra-lean combustion concept to improve the efficiency of SI engine. In SAE WCX Digital Summit 2021 (pp. 1-17). SAE.

[10] Ghorbani A, Steinhilber G, Markus D, Maas U. Ignition by transient hot turbulent jets: an investigation of ignition mechanisms by means of a PDF/REDIM method. Proceedings of the Combustion Institute. 2015; 35(2):2191-8.

[11] Korb B, Kuppa K, Nguyen HD, Dinkelacker F, Wachtmeister G. Experimental and numerical investigations of charge motion and combustion in lean-burn natural gas engines. Combustion and Flame. 2020; 212:309-22.

[12] Validi A, Schock H, Jaberi F. Turbulent jet ignition assisted combustion in a rapid compression machine. Combustion and Flame. 2017; 186:65-82.

[13] Sadanandan R, Markus D, Schießl R, Maas U, Olofsson J, Seyfried H, et al. Detailed investigation of ignition by hot gas jets. Proceedings of the Combustion Institute. 2007; 31(1):719-26.

[14] Tang Q, Sampath R, Marquez ME, Sharma P, Hlaing P, Houidi MB, et al. Optical diagnostics on the pre-chamber jet and main chamber ignition in the active pre-chamber combustion (PCC). Combustion and Flame. 2021; 228:218-35.

[15] Biswas S, Tanvir S, Wang H, Qiao L. On ignition mechanisms of premixed CH_4/air and H_2/air using a hot turbulent jet generated by pre-chamber combustion. Applied Thermal Engineering. 2016; 106:925-37.

[16] Attard WP, Parsons P. A normally aspirated spark initiated combustion system capable of high load, high efficiency and near zero NOx emissions in a modern vehicle powertrain. SAE International Journal of Engines. 2010; 3(2):269-87.

[17] Attard WP, Fraser N, Parsons P, Toulson E. A turbulent jet ignition pre-chamber combustion system for large fuel economy improvements in a modern vehicle powertrain. SAE International Journal of Engines. 2010; 3(2):20-37.

[18] Thelen BC, Toulson E. A computational study of the effects of spark location on the performance of a turbulent jet ignition system. SAE Technical Paper. 2016:1-15.

[19] Bunce M, Blaxill H, Kulatilaka W, Jiang N. The effects of turbulent jet characteristics on engine performance using a pre-chamber combustor. SAE Technical Paper. 2014:1-20.

[20] Jamrozik A, Tutak W, Kociszewski A, Sosnowski M. Numerical simulation of two-stage combustion in SI engine with prechamber. Applied Mathematical Modelling. 2013; 37(5):2961-82.

[21] Hua J, Zhou L, Gao Q, Feng Z, Wei H. Influence of pre-chamber structure and injection parameters on engine performance and combustion characteristics in a turbulent jet ignition (TJI) engine. Fuel. 2021; 283:119236.

[22] Gholamisheeri M, Givler S, Toulson E. Large eddy simulation of a homogeneously charged turbulent jet ignition system. International Journal of Engine Research. 2019; 20(2):181-93.

[23] Gentz G, Thelen B, Gholamisheeri M, Litke P, Brown A, Hoke J, et al. A study of the influence of orifice diameter on a turbulent jet ignition system through combustion visualization and performance characterization in a rapid compression machine. Applied Thermal Engineering. 2015; 81:399-411.

[24] Pielecha I. Numerical investigation of lambda-value prechamber ignition in heavy duty natural gas engine. Combustion Engines. 2020; 182(2):31-9.

[25] Kim J, Scarcelli R, Som S, Shah A, Biruduganti MS, Longman DE. Numerical investigation of a fueled pre-chamber spark-ignition natural gas engine. International Journal of Engine Research. 2022; 23(9):1475-94.

[26] Baratta M, Misul D, Viglione L, Xu J. Combustion chamber design for a high-performance natural gas engine: CFD modeling and experimental investigation. Energy Conversion and Management. 2019; 192:221-31.

[27] Shin J, Choi J, Seo J, Park S. Pre-chamber combustion system for heavy-duty engines for operating dual fuel and diesel modes. Energy Conversion and Management. 2022; 255:115365.

[28] Bigalli S, Catalani I, Balduzzi F, Matteazzi N, Agostinelli L, De LM, et al. Numerical investigation on the performance of a 4-stroke engine with different passive pre-chamber geometries using a detailed chemistry solver. Energies. 2022; 15(14):1-18.

[29] Baratta M, Misul D, Spessa E, Viglione L, Carpegna G, Perna F. Experimental and numerical approaches for the quantification of tumble intensity in high-performance SI engines. Energy Conversion and Management. 2017; 138:435-51.

[30] Muthukumar S, Gunasekaran EJ, Ramesh P, Karthikeyan M. Numerical investigation of a GDI engine with pre-combustion chamber. International Journal of Advanced Technology and Engineering Exploration. 2023; 10(106):1242-59.

[31] Kim WT, Huth KY, Lee JW, Kang KY. Numerical simulation of intake and compression flow in a four-valve pent-roof spark ignition engine and validation with LDV data. Proceedings of the Institution of Mechanical Engineers, Part D: Journal of Automobile Engineering. 2000; 214(4):361-72.

[32] Wan J, Qian L, Qian Y, Zhuang Y, Gong Z, Sun Y, et al. Experimental and numerical investigation of combustion, performance and emission characteristics of a GDI engine using hydrogen-water complementary regulation. Journal of the Energy Institute. 2024; 113:101554.

[33] Prabhakaran P, Ramesh P, Saravanan CG, Loganathan M, Gunasekaran EJ. Experimental and numerical investigation of swirl enhancing grooves on the flow and combustion characteristics of a DI diesel engine. Energy. 2016; 115:1234-45.

[34] Colin O, Truffin K. A spark ignition model for large eddy simulation based on an FSD transport equation (ISSIM-LES). Proceedings of the Combustion Institute. 2011; 33(2):3097-104.

[35] Li Y, Huang Y, Luo K, Liang M, Lei B. Development and validation of an improved atomization model for GDI spray simulations: coupling effects of nozzle-generated turbulence and aerodynamic force. Fuel. 2021; 299:120871.

[36] Li X, Li D, Dimitriou P, Ajmal T, Aitouche A, Mobasheri R, et al. Comparative investigation on macroscopic and microscopic characteristics of impingement spray of gasoline and ethanol from a GDI injector under injection pressure up to 50 MPa. Energy Reports. 2023; 9:1910-8.

[37] Lou D, Wang T, Fang L, Tan P, Hu Z, Zhang Y, et al. Investigation of the combustion and particle emission characteristics of a GDI engine with a 50 MPa injection system. Fuel. 2022; 315:123079.

[38] Gong C, Si X, Wang Y, Liu F. Effect of CO_2 dilution on combustion and emissions of a GDI engine under the peak NOX generation mixture. Fuel. 2021; 295:120613.

[39] Frasci E, Rosa RN, Moreno BP, Arsie I, Jannelli E. Impact of prechamber design and air–fuel ratio on combustion and fuel consumption in a SI engine equipped with a passive TJI. Fuel. 2023; 345:128265.

[40] Lu Y, Qian Y, Zhang D, Chen Y, Pei Y. Parameters optimization of prechamber jet disturbance combustion system—Effect of prechamber volume and fuel injection mass ratios on performance and exhausts in a diesel engine. Fuel. 2024; 373:132360.

[41] Wang B, Xie F, Hong W, Du J, Chen H, Su Y. The effect of structural parameters of pre-chamber with turbulent jet ignition system on combustion characteristics of methanol-air pre-mixture. Energy Conversion and Management. 2022; 274:116473.

S Muthukumar was born in Chidambaram, Tamilnadu, India on 14/01/1982. He is an Assistant Professor in Mechanical Engineering, Faculty of Engineering and Technology (FEAT), Annamalai University (AU), Annamalainagar, India. He obtained his M.E. degree in Thermal Power Engineering from FEAT, AU in 2010 and B.E. degree in Mechanical Engineering from FEAT, AU in 2004. He is a lifetime member of the Indian Society for Technical Education (ISTE).
Email: muthukith@gmail.com

E James Gunasekaran was born in Cuddalore, Tamil Nadu, India on 25/07/1971. He is a Professor in Mechanical Engineering, Faculty of Engineering and Technology (FEAT), Annamalai University (AU), Annamalainagar, India. He completed his Ph.D (Internal Combustion Engine) in 2009 from Indian Institute of Technology – Madras, M.E (Energy Engineering) from Guindy Engineering College in 1997 and B.E (Mechanical) from AU in 1992. He published nineteen international journal papers, five international conference papers, and one national journal paper. His research interests are Emission Reduction in Engines, CFD application for Internal Combustion Engines with openFOAM and Python CFD. He is a member of Society of Automotive Engineering (SAE).
Email: jamesgunasekaran@gmail.com

P Ramesh was born in Chidambaram, Tamilnadu, India on 02/04/1979. He completed his Ph.D. (Mechanical) in March 2016, M.E. (Thermal power) in May 2005 and B.E (Mechanical) in May 2000. These degrees were obtained from Annamalai University, Annamalainagar – 608002, Cuddalore District, Tamilnadu, India. He published papers in Four international conferences, Four international journal as first author, Five international journal as co-author and five national conferences. He is currently interested in the area of Computational Technique for Internal Combustion Engine and Energy. He had gone through the previous work in the area of design and energy. He is a life member of Indian Society of Technical Education (ISTE), and annual member of Society of Automotive Engineering (SAE).
Email: erprlme_2000@yahoo.co.in

Appendix I

S. No.	Abbreviation	Description
1	3D	Three-Dimensional
2	BDC	Bottom Dead Centre
3	CA	Crank Angle
4	CAD	Computer Aided Design
5	CFD	Computational Fluid Dynamics
6	CI	Compression Ignition
7	CO	Carbon Monoxide
8	CO_2	Carbon Dioxide
9	CR	Compression Ratio
10	DI	Direct Injection
11	ECFM	Extended Coherent Flamelet Model
12	GDI	Gasoline Direct Injection
13	HC	Hydrocarbon
14	HRR	Heat Release Rate
15	IGES	Initial Graphics Exchange Specification
16	IMEP	Indicated Mean Effective Pressure
17	MARS	Monotone Advection and Reconstruction
18	MZ-WSR	Multi-Zone Well-Stirred Reactor
19	NO	Nitrogen Oxide
20	NO_x	Oxides of Nitrogen
21	OH-PLIF	Hydroxide - Planar Laser Induced Fluorescence
22	PFI	Port Fuel Injection
23	PISO	Pressure-Implicit with Splitting of Operators
24	RANS	Reynolds Averaged Navier Stokes
25	RCM	Rapid Compression Machine
26	RNG	Re-Normalized Group
27	SI	Spark Ignition
28	SMD	Sauter Mean Diameter
29	TDC	Top Dead Centre
30	THC	Total Hydrocarbon
31	TJI	Turbulent Jet Ignition
32	UD	Upwind Scheme